PET, CT, and MR Image Registration of the Rat Brain and Skull

Juan José Vaquero, *Senior Member, IEEE*, Manuel Desco, Javier Pascau, *Student Member, IEEE*, Andrés Santos, *Senior Member, IEEE*, Injae Lee, Jürgen Seidel, and Michael V. Green

***Abstract*—Spatially registered positron emission tomography (PET), computed tomography (CT), and magnetic resonance (MR) images of the same small animal offer potential advantages over PET alone: CT images should allow accurate, nearly noise-free correction of the PET image data for attenuation; the CT or MR images should permit more certain identification of structures evident in the PET images; and CT images provide *a priori* anatomical information that may be of use with resolution-improving image-reconstruction algorithms that model the PET imaging process. However, image registration algorithms effective in human studies have not been characterized in the small-animal setting. Accordingly, we evaluated the ability of the automated image registration (AIR) and mutual information (MI) algorithms to register PET images of the rat skull and brain to CT or MR images of the same animal. External fiducial marks visible in all three modalities were used to estimate residual errors after registration. The AIR algorithm registered PET bone-to-CT bone images with a maximum error of less than 1.0 mm. The registration errors for PET brain-to-CT brain images, however, were greater, and considerable user intervention was required prior to registration. The AIR algorithm either failed or required excessive user intervention to register PET and MR brain images. In contrast, the MI algorithm yielded smaller registration errors in all scenarios with little user intervention. The MI algorithm thus appears to be a more robust method for registering PET, CT, and MR images of the rat head.**

***Index Terms*—Image reconstruction, positron emission tomography (PET), small animal imaging.**

I. Introduction

IMAGING technologies originally developed for use in human medical diagnosis are rapidly being adapted to imaging small animals such as mice and rats [1]–[6]. Moreover, it has become increasingly apparent that certain combinations of these methods can yield synergistically improved results. The combination of positron emission tomography (PET) and computed tomography (CT), for example, offers the prospect of nearly noise-free attenuation correction of the PET data. This combination might also aid in correcting PET data for other confounding effects, e.g., positron range variations, by providing spatially detailed information about the distribution of mass within an animal. Combined PET and magnetic resonance (MR) images may also improve target identification by virtue of the high soft tissue contrast available with MR.

Before these benefits can be realized, however, the PET, MR, and CT image data must be in spatial registration. While a number of multimodality registration algorithms have been devised and validated in human subjects [7]–[12], comparatively little is known about the performance of these algorithms when applied to PET, CT, or MR images of small animals [13]. Clinical registration methods commonly used in human PET may not perform well in animal studies because of embedded assumptions tailored to human imaging.

Accordingly, we have begun investigating already validated human registration algorithms to establish their accuracy and usefulness in the small-animal setting. As an initial test, we elected to evaluate the automated image registration (AIR) algorithm [8], and the mutual information (MI) algorithm [11] in three different scenarios: 1) high contrast, highly correlated image structures as in bone-to-bone registration of CT with ^{18}F-fluoride PET images; 2) moderate contrast, moderately correlated image structures, as in brain-to-brain registration of CT or MR with ^{18}F-Fluoro-2-Deoxyglucose (FDG) images; and 3) low contrast, poorly correlated image structures, as in CT or MR with PET brain images of enzyme substrates such as ^{18}F-6-Fluoro-L-Metatyrosine (FMT).

II. Materials and Methods

All experiments were carried out in a similar manner using a rat head (adult Sprague-Dawley, 200–300 g, seven animals total) as the imaging target. In each study, the rat was injected intravenously (IV) or intraperitoneally (IP) with the PET radiopharmaceutical (activities between 1 and 5 mCi). Uptake was allowed to occur for 30–90 min with the animal awake and active. At the end of the uptake period, the animal was sacrificed and the head removed intact. Each head was packed snugly into a plastic tube having almost exactly the head diameter (approximately 3 cm). In two experiments, in order to reduce susceptibility artifacts on the magnetic resonance (MR) scans, the empty space around the head was filled with Fomblin (an inert liquid with magnetic properties equivalent to biological tissue) before the tube was sealed. Glass capillary tubes [1.1 mm internal diameter (ID)] and polyethylene tubing (0.76 mm ID) were filled with an ^{18}F solution and taped to the sides of the tube. These line sources (hereafter referred to as "markers") were oriented along and around the tube as shown in Fig. 1. The plastic tubing was bent in several places into an "L" shape, thereby creating easily identified corner reference points.

Manuscript received December 4, 2000; revised June 11, 2001. The work of M. Desco, J. Pascau, and A. Santos was supported in part by the Spanish and Madrid regional government under Grants III PRICIT Comunidad Madrid, FIS 00/36, TIC99-1085-C02, and CM08.1/0049/98.

J. J. Vaquero, J. Seidel, I. Lee, and M. V. Green are with the National Institutes of Health, Bethesda, MD 20892 USA (e-mail: juanjo@nih.gov).

M. Desco and J. Pascau are with the Hospital Universitario Gregorio Marañón, Madrid, Spain (e-mail: desco@mce.hggm.es).

A. Santos is with the Universidad Politécnica de Madrid, Madrid, Spain (e-mail: andres@die.upm.es).

Publisher Item Identifier S 0018-9499(01)08642-7.

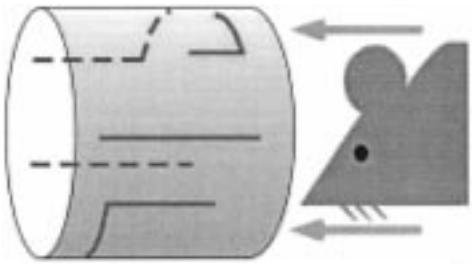

Fig. 1. Marker placement on the external surface of the tube containing the rat head. The L-shaped corners and the ends of the straight markers provide easily identified reference points.

With the head inside and markers attached, the tube was fixed to the mechanical rotation stage of the "piPET" small-animal PET scanner [5]. The head was imaged for several hours in order to acquire large numbers of counts (between 10–44 million counts depending on the study). These data were then reconstructed using the three-dimensional (3-D) OSEM algorithm (20 iterations, five subsets [14]) creating 43 102×102 tomographic images that spanned the 55 mm diameter $\times$ 45 mm high imaging volume of the scanner. The voxel size is $0.55 \times 0.55 \times 1.1$ mm^3, and the spatial resolution in these images is approximately 1.65 mm (isotropic). The reconstructions were done utilizing the high-performance computational capabilities of the Biowulf Cluster at the Center for Information Technology, National Institutes of Health.

Following each PET study, the sample tube was transported to the second modality imaging device. CT images were acquired with a GE High Speed CT/i human CT scanner using the same settings for all studies (80 kVp, 100 mA, $0.2 \times 0.2 \times 1$ mm^3 voxel size). MR images were acquired with a Varian Inova-47 4.7 T using a 3-D gradient-recalled acquisition in the steady state (GRASS) sequence with RF spoiling and gradient crushers ($0.8 \times 0.8 \times 1$ mm^3 voxel size) and a 10-cm internal diameter quadrature bird-cage coil. A GE 1.5 T, using inversion recovery preparation (IRPREP) and 3-D/spoiled GRASS (SPGR) sequences ($0.16 \times 0.16 \times 1.5 - 0.8$ mm^3 voxel size, respectively) and a standard wrist coil, was also used. None of these coils showed any significant inhomogeneity in any image. The whole head was imaged with each modality.

After removing the markers from the PET, MR, and CT volumetric data sets, the studies were registered with the AIR and MI algorithms. The AIR algorithm was employed in a manner previously validated in human clinical studies [15], using a correlation cost function for the CT-^{18}F-fluoride registration and a ratio cost function for the remaining studies.

The MI algorithm was employed with a user-selectable number of subsampling steps: 884, 442, 221, or 111 (XYZ subsampling). Manual prealignment and volume trimming were required before registration. Together, these tasks required about 5 min for each data set. Prealignment consisted of a simple manual reorientation of the volumes so as to place the volumes within the algorithm's "capture" range. Volume trimming (removal of image points not common to both data sets) was required to avoid converging to a false registration solution. However, once the transformation matrix was found, the registration was applied to the original volumes.

TABLE I
FUNCTIONAL PERFORMANCE

Method	18F-CT	FDG-CT	FDG-MR	FMT-MR
AIR	GOOD	Unusable[a]	Unusable[a]	Unusable[a]
MI	GOOD	FAIR[b]	GOOD[b]	GOOD[b]

[a] CT and MR contrast less than optimal.
[b] Pre-alignment and FOV matching required.

TABLE II
REGISTRATION ERRORS MAX (MEAN) IN MILLIMETERS

Method	18F-CT	FDG-CT	FDG-MR	FMT-MR
AIR	1.0 (0.8)	2.4 (2.1)	-	-
MI	0.7 (0.6)	1.4 (1.1)	1.4 (1.1)	1.5 (1.3)

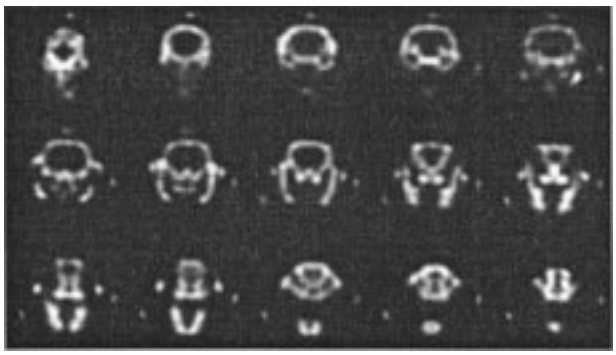

Fig. 2. ^{18}F-fluoride PET transaxial images of the rat head starting at the rear of the skull (top left) and ending at the nose (bottom right). The dots around the head are the reference markers.

In all cases, a rigid geometric transformation (six parameters) was used and no smoothing was applied to the CT, MR, or PET images. Both the AIR and MI algorithms used Powell's convergence optimization method [16].

The output obtained by applying the algorithms consisted of the transformation matrix and the transformed volume, but without estimates of the registration errors. To estimate these errors, the singular value decomposition (SVD) algorithm [17] was applied to 12 to 15 homologous marker pairs identified visually in each data set to determine the "perfect" registration transformation matrix. This transformation was applied to a set of points spaced in and around the rat head. The SVD-transformed set of points was then retransformed with the inverse of the transformation matrix arising from the multimodality registration. The mean Euclidean distance between these final points and the maximum distance between these points were taken as measures of registration accuracy. This method is described in more detail in [18].

In addition to registration accuracy, the "functional performance" of both algorithms was coarsely assessed by recording the amount of user time required to prepare the data sets for registration. If this time was less than 15 min per data set, the algorithm was said to exhibit "good" functional performance; between 15 and 30 min, "fair" functional performance; and more

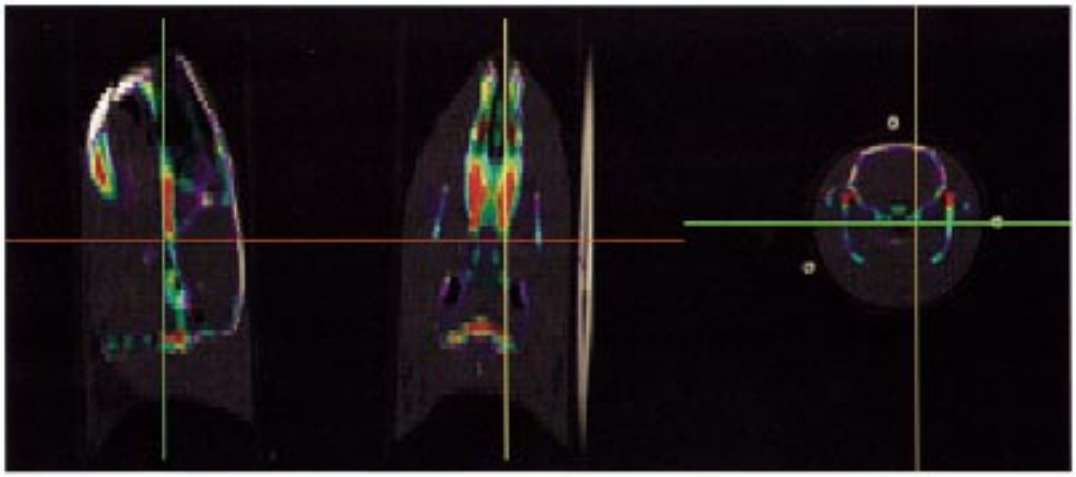

Fig. 3. Overlays of AIR registered ^{18}F-fluoride and CT images of the rat head. The images from left to right are sagittal, coronal, and transaxial sections through the head. The animal is looking toward the top of the figure in the two leftmost images and directly out of the image on the right. Images are displayed using the brightness/hue technique.

than 30 min, "unusable." If an algorithm failed to converge, it was also declared unusable.

Finally, after all preregistration steps had been completed, approximately 1 min was required to obtain a registration solution with the AIR algorithm in the most favorable case (bone-to-bone) and 15 min in the case of CT-^{18}F-FDG brain-to-brain. Other AIR registrations were declared unusable due to the preprocessing time required to prepare the data sets. After all preregistration steps had been completed for the MI algorithm, approximately 20 min were typically required to converge to a valid solution. All registrations were run on a Pentium-III-type computer using IDL (Research Systems, Inc., Boulder, CO) as the development tool. The kernel of the AIR algorithm, implemented in "C" language, was taken from the LONI software package.[1]

Registered images were portrayed with a brightness/hue technique: the grayscale CT or MR values modulated the brightness of the PET data encoded as a transparent color overlay.

III. Results

A. AIR Algorithm

^{18}F-fluoride PET and CT data sets were treated as an intramodality registration (correlation cost function) since both CT and PET images showed a strong spatial correlation in intensity distributions. The algorithm was relatively insensitive to parameter settings and converged rapidly toward registration (Table I). The maximum registration error within the brain volume (Table II) was 1.0 mm. Transaxial ^{18}F-fluoride PET images of the rat head are shown in Fig. 2 and registered with the corresponding CT images in Fig. 3.

The algorithm was unstable when registering ^{18}F-FDG PET and CT and did not converge until all nonbrain structures were removed from both studies, a process requiring extensive user interaction. For the algorithm to converge, it was necessary to segment the brain in both modalities by employing a user-driven and supervised semiautomatic segmentation algorithm (region growing plus manual editing).

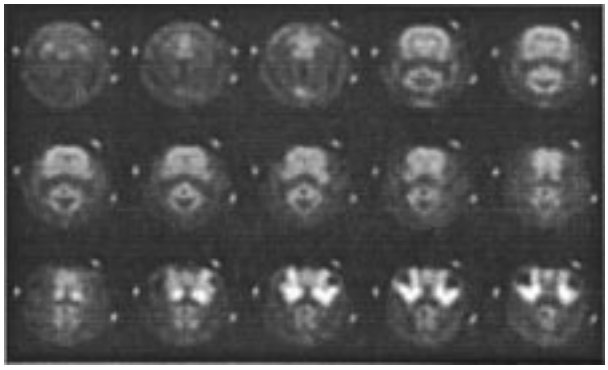

Fig. 4. ^{18}F-FDG transaxial slices starting from the rear of the skull (top left) and ending at the rat eyes (bottom right). The external bright dots are the capillary tubes used as reference markers. Bright comma-shaped structures in the lower right images are the Harderian glands that partially englobe each eye.

The registration algorithm was then applied not to the original gray-value images but to the homogeneous regions obtained from this segmentation procedure. The maximum registration error after these labor intensive manipulations was 2.4 mm with an average error of 2.1 mm (Table II). Even larger errors or a failure to converge were encountered when attempting to register the FDG and MR images. Consequently, the AIR algorithm was declared "unusable" in the MR application due to the extensive preprocessing required, and attempts to refine the registration process further were abandoned. As a result, registration errors are not included for the MR registrations in Table II.

B. MI Algorithm

Data sets registered with the MI algorithm yielded errors close to the largest dimension (1.1 mm) of the PET voxel size in most cases (Table II). Registration errors between CT and ^{18}F-FDG were 1.4 mm maximum and 1.1 mm mean. Transaxial slices through the rat head labeled with ^{18}F-FDG are shown in Fig. 4 and registered with the corresponding MR images in Fig. 5.

[1]Available at http://bishopw.loni.ucla.edu/AIR3/index.html.

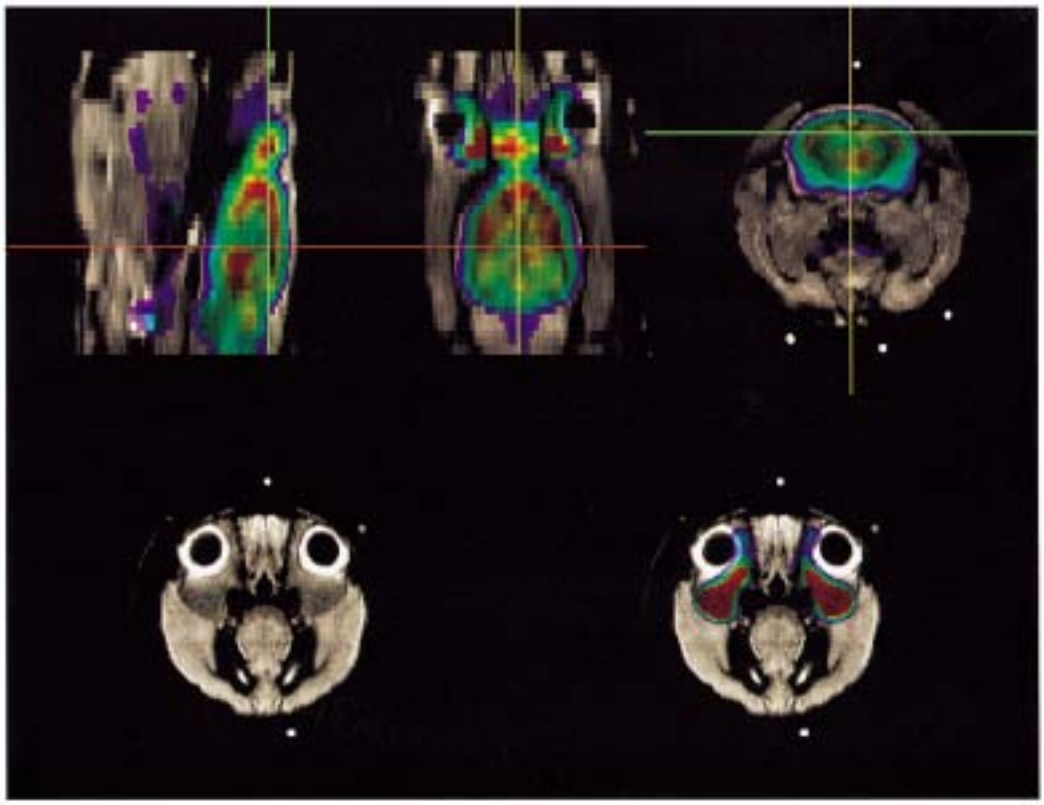

Fig. 5. Upper panel: MI registered sagittal, coronal, and transaxial overlays of ^{18}F-FDG and MR brain images using the brightness/hue technique (see text). Lower panel: transaxial MR image through the eye region (left) registered with the corresponding PET image (right). Note the near perfect match of the Harderian glands seen in the PET image with the glands seen in the MR image.

Selected transaxial slices from an ^{18}F-FMT study of the rat head are shown in Fig. 6. The compound 6-[^{18}F]fluoro-L-metatyrosine (6-FMT) accumulates preferentially in the caudate putamen, visible as two bright regions in several consecutive images. Although these two structures can be clearly identified in the images, there are no other visible landmarks to help identify their exact position inside the brain. The result of registering these images with the corresponding MR images is shown in Fig. 7. Registration errors in this case (Table II) were 1.5 mm maximum and 1.3 mm mean. As noted above, this result was obtained with only modest user intervention (Table I).

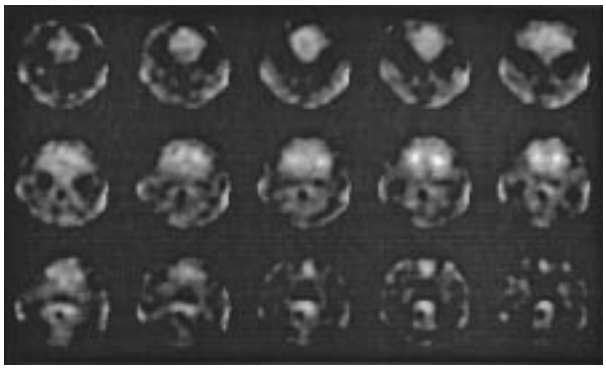

Fig. 6. ^{18}F-FMT PET transaxial images starting from the rear of the skull (top left) and ending at the rat nose (bottom right). The external markers have been removed by masking. The two bright regions in the middle row right are the caudate putamen.

IV. Discussion

There is growing interest in performing multimodality imaging studies in small experimental animals. If the potential of such studies is to be realized, however, methods must be devised whereby the results of each modality can be interpreted in relation to the other modalities at every point in their conjoint imaging space. Registration algorithms based on markers, either clearly defined internal landmarks or external references attached to the sample, allow accurate image registration without assumption about image content. However, internal markers are not always evident in images obtained by different modalities, and external markers can interfere with the experimental design or have other practical disadvantages, e.g., how to attach them rigidly to a living animal.

Multimodality image registration methods developed for human use may be a convenient means of achieving satisfactory registration provided that accuracy remains high and user intervention low when applied to small animals. This study was undertaken with the entirely practical goal of assessing the ability of two already validated human registration algorithms to accurately and easily register PET images of the rat head with corresponding MR and CT images. Although this combination of target and modalities is a small subset of possible imaging combinations, PET combined with these particular modalities offers several significant advantages over PET brain imaging alone. For example, registered PET and MR images of the rat

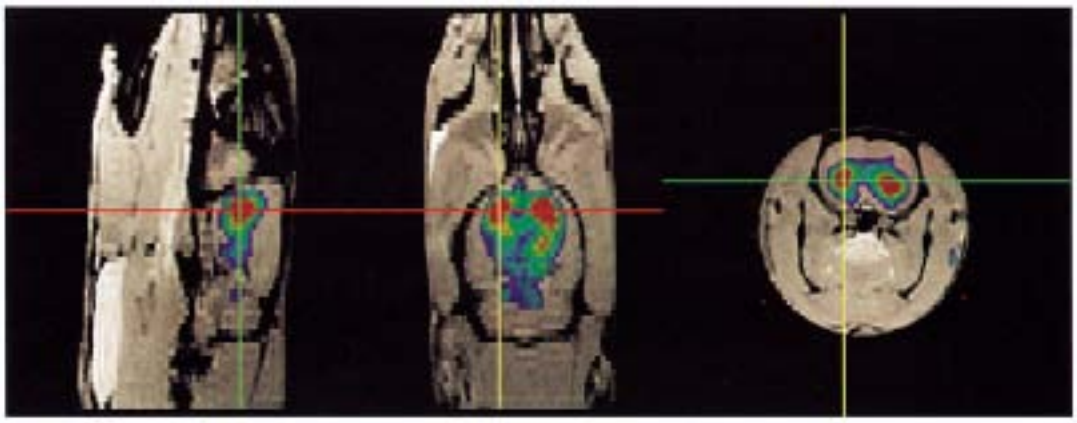

Fig. 7. Overlays of MI registered sagittal (left), coronal (center), and transaxial (right) ^{18}F FMT and MR brain images using the brightness/hue technique. Placement of the PET caudate putamen in these images corresponds to the known location of these structures in the rat brain (anterior and left–right centered). Animal is in the same orientation as in Fig. 3.

head should improve the accuracy of identifying structures labeled with the PET radiopharmaceutical. In the PET/MR registration shown in Fig. 5, for example, it is clear that the high FDG concentration seen in Fig. 4 is not in the eyes or some anterior brain structure but rather in the Harderian glands seen in the MR images. Registered PET and CT images, such as those shown in Fig. 3, should also allow nearly noise-free correction of the PET image data for attenuation and, potentially, provide additional *a priori* information useful in improving PET image quality.

The two algorithms perform differently depending on the data sets to be registered. The AIR algorithm assumes that the data present in the two image sets possess spatially and intensity correlated grayscales. In particular, a given tissue must show homogeneous gray values in both modalities, and two tissues with different gray levels in one modality should not show the same level in the other modality. Since the PET and CT bone images closely approximate this requirement, it would be expected that the bone-to-bone registration would be accurate and require little, if any, user intervention (as was the case). On the other hand, the AIR algorithm could not be used without substantial user intervention in brain-to-brain registrations, providing results with increased registration errors. The reason for this is, in part, that the AIR algorithm, developed for human use, cannot account for the presence of the Harderian glands and other extracerebral structures in the rat head. The Harderian glands are not present in human subjects but in the rat (and other rodents) concentrate ^{18}F-FDG more strongly than the brain. Unless these structures are removed by segmentation (not a simple task in the case of rodent heads), the AIR algorithm cannot converge as it does when registering cross-modality images of human heads. Thus, it is likely that registration methods based on assumptions like those underlying the AIR algorithm will typically require additional segmentation steps to eliminate extreme anatomical and/or functional differences that exist between humans and small animals while incurring larger registration errors.

The MI algorithm, on the other hand, does not assume spatially correlated grayscales. Instead, the MI method seeks to maximize mutual information [11] of the two data sets during registration. The results shown in Table II and in the sample images imply that this approach is more robust and does not require highly correlated image structures to yield accurate registrations, at least in the three cases tested. To achieve these results, however, the data sets required manual prealignment and volume trimming prior to registration. Although the prealignments do not need to be accurate, without these interventions the algorithm would sometimes fail to converge or would converge to an inaccurate registration. Because of these requirements, the MI algorithm could not be implemented as a fully "automatic" method. On the other hand, these two preprocessing steps required only about 5 min to complete for each data set. As implied above, user verification of a successful alignment was also required. The dependency of the registration accuracy on the manual prealignment precision was not evaluated and may require further investigations.

This study is limited in several respects. First, the quality of the CT and MR rat-head images was not optimal. The CT images were obtained with a human CT scanner operating at 80 kVp, a value that could not be reduced. Tissue contrast in the head and brain could be improved if a lower setting were permitted. CT scanners specifically designed for small-animal imaging and operating at lower tube voltages [3] exhibit appreciably higher tissue contrast and could, therefore, potentially yield improved image registration compared to that observed in this work. The MR image contrast might also be improved with a similar effect on registration accuracy. With the MR instruments available for this study, contrast could only be improved at the expense of spatial resolution. Since a high spatial resolution was required to visualize structures in the rat brain and head, contrast was lower than might otherwise have been desirable. MR systems designed for small-animal imaging overcome this problem by operating at higher field strengths, by using different coils and pulse sequences, and by imaging for longer times [19]. The use of such higher contrast images could affect registration accuracy, as in the CT case above.

This study is restricted to multimodality registration of images of a motionless rat head unchanged from one imaging session to the next. Moreover, the PET images were of very high statistical quality due to the extended periods of PET data acquisition. While both of these conditions were necessary to test the

inherent performance of the two registration algorithms, they rarely occur in real imaging studies. If different modality images of the head are obtained at different times in a living animal, changes can occur in the target that can potentially confound image registration. For example, attempts to register bone images of the head over time could be adversely affected by changes in the position of the lower jaw from one session to the next. While such changes could be edited out by segmentation, additional user intervention is required and the registration process made more complex. Animal movement during each imaging study could also degrade registration accuracy by blurring together structures important to the registration process.

The statistical quality of PET images may also affect the performance of these algorithms. It would be expected that as statistical quality deteriorates, the ability of either algorithm to produce accurate registrations would decrease. It is also likely that the two algorithms are not equally affected by statistical variations. Since statistical quality in real studies is often highly variable and generally poorer than in this work, the relationship between statistical precision and registration accuracy needs to be examined directly by experiment.

V. Conclusions

The AIR algorithm, developed for use in multimodality image registration in human subjects, can be used to automatically register CT with ^{18}F-fluoride bone images of the rat head. PET ^{18}F-FDG images of the brain can also be registered with CT but only after modifications that require extensive user intervention accompanied by larger registration errors. The AIR algorithm was declared unusable when attempting to register MR and PET images of the rat head due to the excessive amount of time required to prepare the data sets for registration.

The MI algorithm, though unable to operate automatically, yielded more accurate registrations with modest user intervention in all imaging scenarios. The MI algorithm thus appears to offer advantages over the AIR algorithm when registering PET images of the rat head with corresponding MR and CT images.

Acknowledgment

The authors thank W. Eckelman and E. Jagoda for their assistance in preparing the animal samples; C. Johnson for his support with the OSEM reconstructions; M. Skopec for her assistance with the CT acquisitions; and J. Frank, B. Lewis, A. Olson, and P. Van Gelderen for their help with the MR studies.

References

[1] M. Ivanovic, D. A. Weber, and S. Loncaric, "Design of rotating multipinhole SPECT system for high resolution small animal imaging," *J. Nucl. Med.*, vol. 39, pp. 174P–174P, 1998.

[2] A. P. Jeavons, R. A. Chandler, and C. A. R. Dettmar, "A 3D HIDAC-PET camera with sub-millimeter resolution for imaging small animals," *IEEE Trans. Nucl. Sci.*, vol. 46, pp. 468–473, 1999.

[3] M. J. Paulus, H. Sari-Sarraf, S. S. Gleason, M. Bobrek, J. S. Hicks, and D. K. Johnson *et al.*, "A new X-ray computed tomography system for laboratory mouse imaging," *IEEE Trans. Nucl. Sci.*, vol. 46, pp. 558–564, 1999.

[4] A. F. Chatziioannou, S. R. Cherry, Y. Shao, R. W. Silverman, K. Meadors, and T. H. Farquhar *et al.*, "Performance evaluation of microPET: A high-resolution lutetium oxyorthosilicate pet scanner for animal imaging," *J. Nucl. Med.*, vol. 40, pp. 1164–1175, 1999.

[5] S. Siegel, J. J. Vaquero, L. Aloj, J. Seidel, W. R. Gandler, and M. V. Green, "Initial results from a PET/planar small animal imaging system," *IEEE Trans. Nucl. Sci.*, vol. 46, pp. 571–575, 1999.

[6] M. V. Green, J. Seidel, J. J. Vaquero, E. Jagoda, I. Lee, and W. C. Eckelman, "High resolution PET, SPECT and projection imaging in small animals," *Comput. Med. Imaging Graph.*, vol. 25, pp. 79–86, 2001.

[7] C. A. Pelizzari, G. T. Y. Chen, D. R. Spelbring, R. R. Weichselbaum, and C. T. Chen, "Accurate 3-dimensional registration of CT, PET, and or MR images of the brain," *J. Comput. Assist. Tomog.*, vol. 13, pp. 20–26, 1989.

[8] R. P. Woods, J. C. Mazziotta, and S. R. Cherry, "MRI-PET registration with automated algorithm," *J. Comput. Assist. Tomog.*, vol. 17, pp. 536–546, 1993.

[9] B. A. Ardekani, M. Braun, B. F. Hutton, I. Kanno, and H. Iida, "A fully-automatic multimodality image registration algorithm," *J. Comput. Assist. Tomog.*, vol. 19, pp. 615–623, 1995.

[10] W. M. Wells, P. Viola, H. Atsumi, S. Nakajima, and S. Kikinis, "Multi-modal volume registration by maximization of mutual information," *Med. Image Anal.*, vol. 1, pp. 35–51, 1996.

[11] F. Maes, A. Collignon, D. Vandermeulen, G. Marchal, and P. Suetens, "Multimodality image registration by maximization of mutual information," *IEEE Trans. Med. Imaging*, vol. 16, pp. 187–198, 1997.

[12] C. Studholme, D. L. G. Hill, and D. J. Hawkes, "An overlap invariant entropy measure of 3D medical image alignment," *Pattern Recognit.*, vol. 32, pp. 71–86, 1999.

[13] N. Hayakawa, K. Uemura, K. Ishiwata, Y. Shimada, N. Ogi, and T. Nagaoka *et al.*, "A PET-MRI registration technique for PET studies of the rat brain," *Nucl. Med. Biol.*, vol. 27, pp. 121–125, 2000.

[14] C. A. Johnson, J. Seidel, R. E. Carson, W. R. Gandler, A. Sofer, and M. V. Green *et al.*, "Evaluation of 3D reconstruction algorithms for a small animal PET camera," *IEEE Trans. Nucl. Sci.*, vol. 44, pp. 1303–1308, 1997.

[15] M. Desco, J. López, C. Benito, A. Santos, P. Domínguez, and S. Reig *et al.*, "A multimodality workstation in practice," in *Computer Assisted Radiology and Surgery (CARS'99)*, H. U. Lemke, M. W. Vannier, K. Inamura, and A. G. Farman, Eds. Amsterdam, The Netherlands: Elsevier Science, 1999, pp. 218–222.

[16] W. H. Press, S. A. Teukolsky, W. T. Vetterling, and B. P. Flannery, *Numerical Recipes in C*, 2nd ed. Cambridge, U.K.: Cambridge Univ. Press, 1992, pp. 412–420.

[17] K. S. Arun, T. S. Huang, and S. D. Blostein, "Least squares fitting of two 3D point sets," *IEEE Trans. Pattern Anal. Image Recogn.*, vol. 9, pp. 699–700, 1987.

[18] J. West, J. M. Fitzpatrick, M. Y. Wang, B. M. Dawant, C. R. Maurer, and R. M. Kessler *et al.*, "Comparison and evaluation of retrospective intermodality brain image registration techniques," *J. Comput. Assist. Tomog.*, vol. 21, pp. 554–566, 1997.

[19] M. Rivera, J. J. Vaquero, A. Santos, J. Ruiz-Cabello, and F. del Pozo, "MRI visualization of small structures using improved surface coils," *Magn. Res. Imaging*, vol. 16, pp. 157–166, 1998.